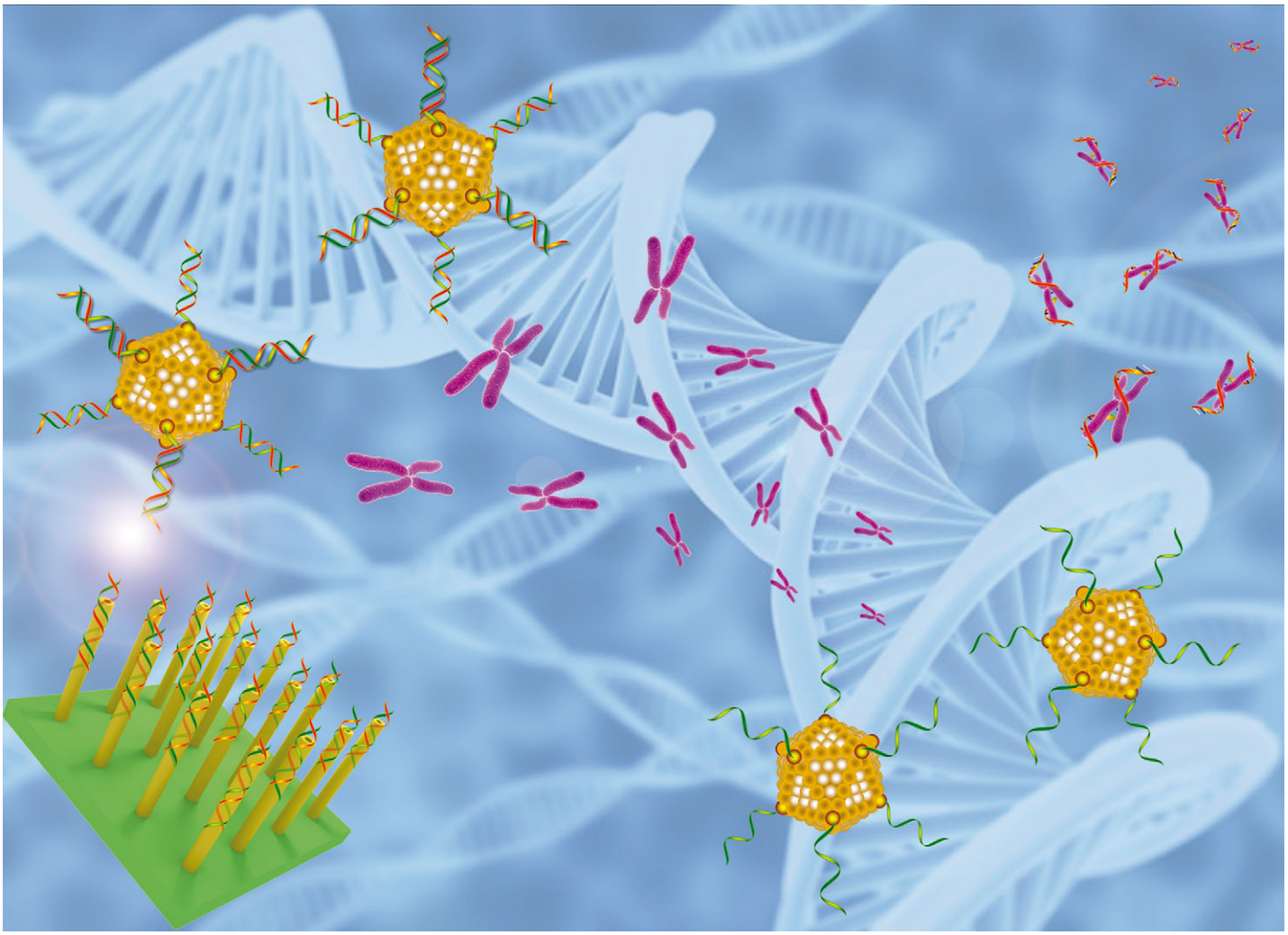

Showcasing research from Prof. Wanqin Jin's group, State Key Laboratory of Materials-Oriented Chemical Engineering, College of Chemistry and Chemical Engineering, Nanjing Tech University, P. R. China.

Facile fabrication of a three-dimensional gold nanowire array for high-performance electrochemical sensing

A three-dimensional gold nanowire array (3D GNA) was successfully prepared with a facile template-assisted approach in this work. Based on the proposed 3D GNA, a novel aptasensor was constructed with a general sensing strategy, and as an example, excellent performance was observed in the assay of thrombin.

As featured in:

See Wanqin Jin *et al.*, *J. Mater. Chem. B*, 2015, **3**, 3134.

ROYAL SOCIETY OF CHEMISTRY

www.rsc.org/MaterialsB

Registered charity number: 207890

Journal of
Materials Chemistry B

PAPER

View Article Online
View Journal | View Issue

Cite this: J. Mater. Chem. B, 2015, 3, 3134

Facile fabrication of a three-dimensional gold nanowire array for high-performance electrochemical sensing†

Lei Shi, Zhenyu Chu, Yu Liu and Wanqin Jin*

Received 6th February 2015,
Accepted 11th March 2015

DOI: 10.1039/c5tb00266d

www.rsc.org/MaterialsB

Great challenges remain in the template-assisted fabrication of metal nanowire arrays on substrates, because enormous effort is required to address the adhesion issues between substrates and adopted templates, *e.g.* anodic aluminum oxide (AAO). Therefore, novel and promising templates are highly desired for the construction of proposed structures. Here, vertical 1,5-diaminoanthraquinone (DAAQ) nanowires were prepared *in situ* on substrates by a facile method, and these were proven to be a reliable and alternative template for the preparation of a metal nanowire array. As an example, with the wet chemical reduction of $HAuCl_4$, a three-dimensional gold nanowire array (3D GNA) was successfully obtained with a DAAQ template. The proposed 3D GNA has an extremely large roughness factor of *ca.* 15, as well as high stability and a favorable surface structure for the diffusion of analytes, making it a suitable candidate for the construction of high-performance electrochemical biosensors. As a result, an ultrasensitive aptasensor was constructed for the detection of thrombin, with a general sensing scheme. The fabricated aptasensor displays an impressively ultralow detection limit of 3 fM (S/N = 3) with a wide linear response from 10 fM to 1 nM, as well as excellent selectivity, good reproducibility and acceptable stability. Further, the biosensor exhibits potential for application in the analysis of real serum samples. The developed DAAQ nanowires are envisaged to become a general template for the fabrication of more nanowire arrays and the as-synthesized 3D GNA could open up a wide range of possibilities for potential applications in biological sensing.

Introduction

Aptamers, a special category of oligonucleotides, play an important role in molecular recognition due to their high affinity and specificity towards extensive targets, *e.g.* metal ions, biological proteins and cells.[1–3] The development of sensitive, selective and rapid aptamer biosensors (aptasensors) has attracted enormous interest in disease diagnosis and biomedical applications. Recently, various aptasensors have been successfully constructed, and these are mainly focused on the analysis of adenosine triphosphate, thrombin, prostate specific antigen, lysozyme, platelet-derived growth factor and angiogenin.[4–11] Several techniques including fluorescence,[12,13] colorimetry,[14] field-effect transistors (FETs)[15] and electrochemistry[16] have been introduced in the construction of aptasensors. Considering the advantages of simplicity, low cost, portability, and particularly easy miniaturization, the electrochemical method has become one of the most attractive techniques in the development of aptasensors.

In general, the concentrations of many crucial analytes are at ultralow levels in biological samples during the early stages of disease progress. To realize opportune and ultrasensitive electrochemical monitoring of related analytes, the development and construction of versatile electrode materials is considered a critical strategy.[17–19] The emerging gold nanomaterials have received significant attention in the fabrication of electrochemical biosensors due to their unique physical and chemical properties, large surface area and excellent biocompatibility.[20–22] Among the multitudinous gold structures, three-dimensional gold nanowire arrays (3D GNAs) have attracted special interest in the electrochemical assay of various analytes, *e.g.* oligonucleotides, glucose and H_2O_2.[23–26] The significantly enlarged surface area of 3D GNAs increases the number of immobilization positions for biomolecules and provides more electrocatalytic sites, contributing to the enhanced acquisition of electrochemical signals and finally improving the sensing performance. To create such GNA structures, templates of anodic aluminum oxide (AAO) and porous polycarbonate (PC) are usually employed. In particular, specialized procedures are required to enhance the interfacial adhesion strength between templates and substrates, in which a thin

State Key Laboratory of Materials-Oriented Chemical Engineering, College of Chemistry and Chemical Engineering, Nanjing Tech. University, Nanjing 210009, P. R. China. E-mail: wqjin@njtech.edu.cn; Fax: +86-25-8317-2292; Tel: +86-25-8317-2266

† Electronic supplementary information (ESI) available. See DOI: 10.1039/c5tb00266d

metal layer is generally sputtered at the bottom of the templates, or the templates are simply placed and tightly fixed on the substrates.[27,28] However, a critical drawback to these methods is that once the templates are removed, most fabricated nanowires collapse or stack due to existing surface tension and poor adhesion strength, which severely restricts and impairs the availability of their surface area. To address this issue, Byun *et al.* fabricated a well-defined GNA on various substrates, in which they introduced a functional polymer layer on the substrates for favourable adhesion with AAO.[29] Further, Ramulu *et al.* developed a two-step electrodeposition method and successfully prepared a vertical GNA with a PC template.[30] Nevertheless, additional and complex treatments on adopted substrates or templates can increase their fabrication cost and hinder their wide application in practice. Therefore, the fabrication of desired 3D GNAs through a facile and reliable method remains a great challenge.

Thrombin (Tob) is an extracellular serine protease and plays crucial roles in the blood coagulation cascade, thrombosis and haemostasis, which is thought to be closely related to a number of cardiovascular diseases, and even the activation and proliferation of cancer cells.[31] To realize a sensitive assay of Tob, various gold nanomaterials including gold nanowires,[32] fractal gold structures,[21] and gold nanoparticles[33] have been applied recently. However, until now few reports have been dedicated to constructing electrochemical Tob aptasensors based on promising 3D GNAs.

In this work, vertical organic nanowires were fabricated *in situ* on a gold electrode through a facile physical vapor transport method, which could conveniently and directly serve as a promising template for the fabrication of a versatile nanowire array. As an example, a novel 3D GNA was successfully prepared with the template, and this possessed an extremely large surface area and could significantly increase the number of immobilization positions for biological probes. In particular, each gold nanowire was separated at a proper distance, facilitating the diffusion of analytes and making them easily accessible to the electrode surface. Here, Tob was selected to demonstrate the superior ability of the GNA in sensing applications. Accordingly, an electrochemical Tob aptasensor was constructed with a general sensing scheme, in which excellent performance as well as a fascinating application for real serum samples was observed.

Experimental section

Chemicals and materials

Hydrogen tetrachloroaurate(III) ($HAuCl_4 \cdot 3H_2O$, 99.9%) was obtained from Alfa Aesar, and gold nanoparticles (AuNPs) with 10 nm diameter were purchased from Strem Chemicals. Thrombin (Tob), lysozyme (Lzm), bovine serum albumin (BSA), hemoglobin (Hb), immunoglobulin G (IgG), 6-mercapto-1-hexanol (MCH), ethylenediaminetetraacetic acid (EDTA, 99%), tri(2-carboxyethyl) phosphine hydrochloride (TCEP, 98%), hexaammineruthenium(III) chloride (RuHex), 1,5-diaminoanthraquinone (DAAQ), polyvinylpyrrolidone (PVP, M_w 3500) and tris(hydroxymethyl)aminomethane (Tris-base) were obtained from Sigma-Aldrich. Here, EDTA was used to sequester multivalent ions and keep them away from the oligonucleotide molecules, making them more stable in the solution.[34] TCEP was used to cleave the S–S bond and activate thiolated oligonucleotides.[35] All oligonucleotides were synthesized by TaKaRa biotechnology Co., Ltd (Dalian, China), and their base sequences were as follows. Capture probe: 5′-SH-$(CH_2)_6$-CGC TAC GAA GAG TCA CCC CAA CCT GCC-3′. The aptamer for Tob (Apt-T): 5′-AGT CCG TGG TAG GGC AGG TTG GGG TGA CT-3′. Reporter probes of Tob (Rp-T): 5′-SH-$(CH_2)_6$-AGG TTG GGG-3′ (Rp-T I) and 5′-SH-$(CH_2)_6$-GAG AAA GAG-methylene blue (MB)-3′ (Rp-T II). Other chemicals employed were all of analytical grade and triple-distilled water was used throughout.

Apparatus

The morphology of the 3D GNA was observed by field-emission scanning electron microscopy (FESEM, Hitachi S4800), and the chemical composition of the GNA was determined by energy-dispersive X-ray spectroscopy (EDX, Hitachi S4800). X-ray diffraction (XRD) was performed on an X-ray diffractometer (D/MAX 2500 V/PC) with a Cu Kα line (0.15419 nm). All electrochemical measurements were performed with a CHI 660C electrochemical workstation (Shanghai Chenhua, China). A three-electrode system consisting of the GNA working electrode, a platinum auxiliary electrode, and an Ag/AgCl (saturated KCl) reference electrode was used.

Fabrication of the 3D GNA on a gold electrode

Vertical DAAQ nanowires were prepared *in situ* by a physical vapor transport method following a known procedure.[36] Briefly, 5 mg of DAAQ powder was first dissolved with 20 mL of ethanol in a 100 mL 2-necked flask, which was then put into a silicon oil bath. Afterwards, the temperature was increased to 60 °C to evaporate the ethanol and the flask was rotated to obtain a thin coating of DAAQ. Then the bare gold electrode was perpendicularly mounted in order to suspend it on top of the flask. The oil bath was subsequently heated to 160 °C for 10 min to vaporize the DAAQ powder. The DAAQ vapor condensed on the gold electrode and vertical nanowires were formed. Finally, the DAAQ nanowire-modified electrode was treated with ion sputtering apparatus with a gold target for 3 s to enhance the binding strength between the DAAQ nanowires and the gold electrode.

Wet chemical reduction was introduced to fabricate the 3D GNA. A precursor solution consisting of 10 mL of water, 0.2 mL of PVP solution (2.5% in water), 1 mL of KI (0.2 M), 0.5 mL of ascorbic acid (0.05 M), and 0.1 mL of $HAuCl_4$ (0.5 M) was prepared first.[37] Then the electrode modified with DAAQ nanowires was dipped into the precursor solution for 20 min, followed by sufficient treatment with hot ethanol to remove the template of organic nanowires. Subsequently, the obtained 3D GNA was cycled in 0.5 M H_2SO_4 aqueous solution to remove any residual impurities. Finally, the freshly cleaned GNA was dried with nitrogen gas and served for the immobilization of capture probes.

Construction of the 3D GNA-based aptasensor for the detection of Tob

Rp-T–AuNP conjugates were introduced to enhance the signal responses. These were prepared through immobilizing Rp-T on

AuNPs.[35] Firstly, 1 mL of AuNPs was centrifuged and the precipitates were resuspended in 1 mL of 10 mM phosphate-buffered saline (PBS, pH 7.4). Then, 0.1 mL of Rp-T in sterilized water with 10 mM TCEP was added to 1 mL of AuNPs and incubated at 4 °C for 16 h. The concentrations of Rp-T I and Rp-T II were 0.1 μM and 1 μM, respectively. Then the Rp-T–AuNP conjugates were aged by gradually adding 2 M NaCl every 30 min to reach a final salt concentration of 0.1 M NaCl. The mixed solution was incubated for another 48 h and finally the solution was centrifuged for 30 min at 4 °C with the supernatant being removed. The red oily precipitate was washed with 10 mM PBS, recentrifuged, and then redispersed in 1 mL of 10 mM PBS.

The freshly cleaned GNA was immersed in an immobilization buffer (pH 7.4) of 10 mM Tris-HCl, 1 mM EDTA, 10 mM TCEP, and 0.1 M NaCl containing 5 μM capture probes and 500 nM MCH for 6 h. Then it was dipped into the hybridization buffer (pH 7.4) of 10 mM PBS, 1 mM EDTA, and 0.25 M NaCl containing 5 μM Apt-T for 3 h. After the hybridization, the oligonucleotide-modified GNA was extensively rinsed with washing buffer (W-buffer, 10 mM Tris-HCl, pH 7.4). Afterwards, the GNA was immersed in solutions of Tob of various concentrations for 2 h, again followed by thoroughly washing with the W-buffer. Finally, 0.1 mL of Rp-T–AuNPs was added into the detection system for 2 h at 37 °C.

Quantitative detection of Tob in human serum

Healthy human serum was used in this work, which was previously subjected to centrifugation for 15 min (12 000*g*). The serum centrifugation ultrafiltrate was used for the following measurements. The concentration of Tob in the blank serum sample was first detected by the obtained calibration curve of the fabricated aptasensor, and the background signal could be subtracted in the subsequent quantitative detection. Then standard solutions of Tob with different concentrations were added into the 100× diluted serum and electrochemical measurements were performed.

Electrochemical measurements

Cyclic voltammetry (CV) was carried out at a scan rate of 100 mV s^{-1}, square wave voltammetry (SWV) was recorded at a frequency of 5 Hz, electrochemical impedance spectroscopy (EIS) was performed with the frequency ranging from 0.01 Hz to 100 kHz with a signal amplitude of 5 mV, and chronocoulometry (CC) was conducted at a pulse width of 0.25 s. The electrolyte for CV and SWV was 10 mM PBS with 0.25 M NaCl (pH 7.4), for CC it was 10 mM Tris-HCl (pH 7.4), and for EIS it was 5 mM $K_3[Fe(CN)_6]/K_4[Fe(CN)_6]$ with 0.1 M KCl. During the CC measurement, a nitrogen atmosphere was maintained in the electrochemical cell.

Results and discussion

Characterization of the fabricated 3D GNA

As shown in Fig. 1A and B, vertical DAAQ nanowires with a length of 2.5 μm and diameter of *ca.* 120 nm were formed *in situ* on the bare gold electrode, which directly served as a template to prepare the metal nanowire array. As is well known, the anionic $AuCl_4^-$ has a high affinity to amino groups due to electrostatic and coordinate interactions. Therefore, the amino groups present in the DAAQ molecules would promote the chemical adsorption of $HAuCl_4$, resulting in the formation of densely packed gold nanoparticles around the DAAQ nanowires after reduction. Fig. 1C and D present a uniformly distributed 3D GNA, which was prepared with an appropriate time of 20 min in the precursor solution. It should be noted that the obtained nanowires were approximately separated at a proper distance, in order to facilitate the diffusion of analytes at the electrode surface.[38] With a high magnification focused on the surface of the obtained gold nanowire, it could be seen that gold nanoparticles were closely spaced along the surface, and a gold nanowire with a diameter of *ca.* 300 nm was prepared (Fig. 1E). As shown in Fig. 1F, after thoroughly removing the DAAQ template a hollow gold nanowire was observed, which would promote electron transfer and realize the good conductivity of the proposed 3D GNA. In addition, the effect of reaction time in the precursor solution on the morphologies of the obtained gold nanowires was investigated (as shown in Fig. S1 in the ESI†). When a reaction time of 10 min was adopted, fewer gold particles were reduced on the DAAQ nanowire template, leading to the collapse of the array structure once the template was removed. If a longer reaction time of 30 min was implemented, the formed gold nanowires continued to grow and the over-long nanowires tended to bend and interlace with each other. It is worth mentioning that gold nanowires with a sparse density would not give the desired large surface area, while interlaced structures would hinder the diffusion of analytes at the interfaces, both of which would severely limit their potential applications in electrochemical sensing.

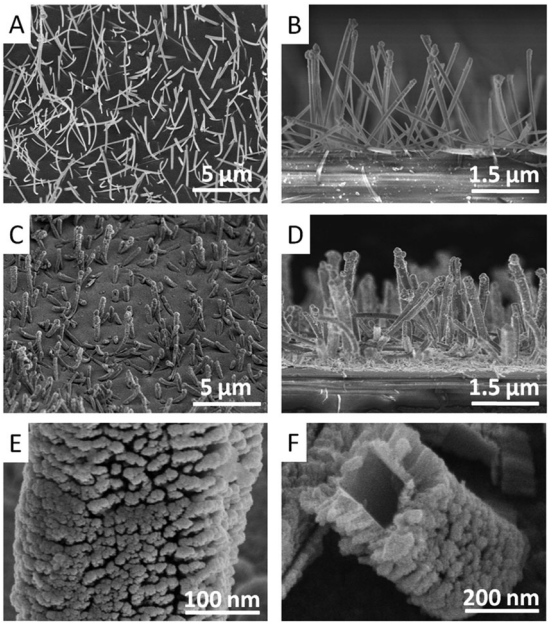

Fig. 1 FESEM images of: (A) vertical DAAQ nanowires, (B) cross-sectional view of DAAQ nanowires, (C) the fabricated 3D GNA, (D) cross-sectional view of the 3D GNA, (E) magnified view of a single gold nanowire, (F) a hollow gold nanowire after removing the DAAQ template.

Meanwhile, the surface properties and chemical composition of the fabricated 3D GNA were explored with XRD and EDX. The powder XRD pattern for the GNA is shown in Fig. 2A, and it

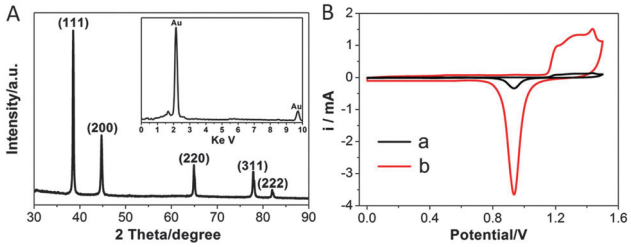

Fig. 2 (A) Powder XRD pattern of the proposed 3D GNA, inset is the EDX spectrum. (B) CVs of (a) the bare gold electrode, (b) the 3D GNA in 0.1 M H_2SO_4 solution.

is evident that the characteristic peaks belong to fcc Au. The peaks located at around 38.0, 44.2, 64.5, 77.5 and 81.7° are assigned to the (111), (200), (220), (311) and (222) surfaces, respectively. Obviously, the intensity ratio of the {111} to the {200} diffraction line (2.3) is higher than that in the standard diffraction pattern of gold powder (1.9), indicating that the proposed gold nanowire structure has a tendency to grow along the lowest energy {111} surface.[39] The inset in Fig. 2A is the EDX spectrum; it is obvious that the gold element has became the dominating component of the obtained GNA, demonstrating that the DAAQ template was sufficiently removed after treating with hot ethanol, which is consistent with the result shown in Fig. 1F. Moreover, the real surface area of the GNA was electrochemically investigated in 0.1 M H_2SO_4, and the results are shown in Fig. 2B. Gold oxidation started at around 1.2 V, showing three anodic current peaks. As the peak area reflects the relative surface area of the gold electrode, the 3D GNA, possessing a larger surface area than that of a bare gold electrode, shows an obvious oxidation peak in curve b. Subsequently, the formed gold monolayer oxide was electrochemically reduced in the negative potential sweep and the reduction peaks occur at a potential of *ca.* 0.94 V.[40] By integrating the charge required for reducing the gold oxide formed in the positive sweep and assuming that the reduction of a monolayer of gold oxide requires 386 μC cm^{-2}, the real surface area of the GNA was determined to be 1.80 cm^2. Considering that the geometrical area of the bare gold electrode is only 0.12 cm^2, a large roughness factor (R_f, the ratio of real surface area to geometrical area) of the GNA was calculated to be *ca.* 15.

All of these promising features, *e.g.* significantly enhanced surface area, pure component, high stability and favorable surface structure, would make the fabricated 3D GNA a good candidate for the construction of ultrasensitive electrochemical aptasensors.

Design of the 3D GNA-based sensing scheme

A general sensing scheme has been designed in this work, which is shown in Fig. 3. The 5′-thiolated capture probes containing a complementary sequence of Apt-T were firstly immobilized on the GNA through the Au–S bond. To improve the recognition ability of the capture probes, a passivation process was performed by simultaneous reaction with MCH, which optimized the distribution of probes and forced the probes to adopt an upright surface orientation. Then the Apt-T was introduced to

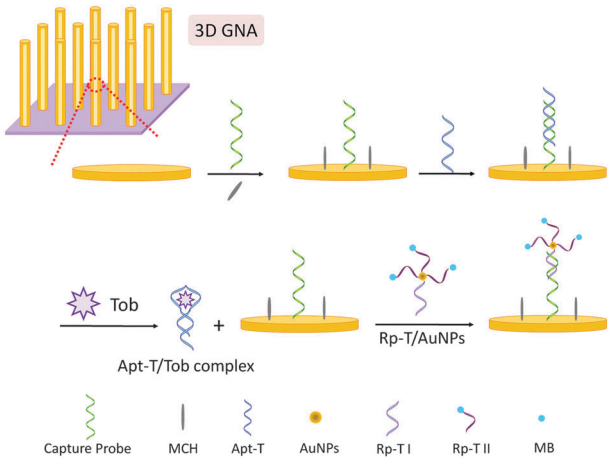

Fig. 3 Schematic illustration of the 3D GNA-based electrochemical aptasensor for the detection of Tob.

sufficiently hybridize with the capture probes. As is well known, duplex strands of DNA molecules with enhanced stability will be produced if more base pairs are formed interiorly.[41] On account of the fact that more base pairs would be formed between capture probes and Apt-T (17) than between capture probes and Rp-T I (9), the capture probes preferred to hybridize with Apt-T and form stable duplex strands. However, as Tob can bind with Apt-T and form a more stable tertiary complex structure than the duplex strands of capture probes and Apt-T,[42] the hybridized Apt-T on the surface was detached from the capture probes in the presence of Tob molecules. As a result, the Apt-T–Tob complex was disassociated from the electrode surface, leading to the exposure of hybridization sites for Rp-T I. Finally, the Rp-T–AuNPs were added into the detection system, in which Rp-T I would hybridize with the capture probes and the electrochemical indicator in the Rp-T II could be effectively used to monitor the concentration of Tob. Undoubtedly, the proposed sensing scheme could be feasibly introduced to construct other electrochemical aptasensors.

Electrochemical characterization of the aptasensor

EIS is an effective approach to investigate the resistance of interfacial electron transfer, and this was implemented to monitor the impedance changes at different interfaces in this work.[43] As shown in Fig. 4A, due to the enlarged electroactive surface and high conductivity of the array structure, the 3D GNA possessed a smaller semicircle (curve a) compared with that of the bare gold electrode (curve b), indicating a low resistance to the redox indicator $[Fe(CN)_6]^{3-/4-}$ in solution. Once the 3D GNA was treated with a mixture consisting of capture probes and MCH, the resistance increased obviously (curve c). As we know, the increased electron transfer resistance may be attributed to two factors: one is the electrostatic repulsion of the oligonucleotide strands with negatively charged phosphate backbones towards the anionic $[Fe(CN)_6]^{3-/4-}$, while the other is the steric hindrance arising from the flexible oligonucleotide strands and organic molecules of MCH. After the hybridization with Apt-T, the electrostatic repulsion and steric hindrance were further enhanced because of the introduction of additional

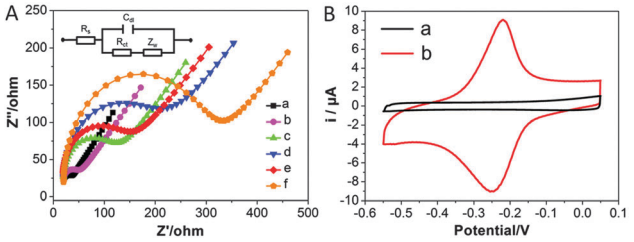

Fig. 4 (A) Nyquist plots in $Fe(CN)_6^{3-/4-}$ solution of the aptasensor at different interfaces: (a) the 3D GNA, (b) the bare gold electrode, (c) capture probes and the MCH-immobilized GNA, (d) after hybridization with Apt-T, (e) after the addition of Tob, (f) in the presence of Rp-T–AuNPs. Z_w in the inset represents the Warburg impedance. (B) CVs in PBS solution: (a) in the absence of Tob, (b) in the presence of 1 nM Tob.

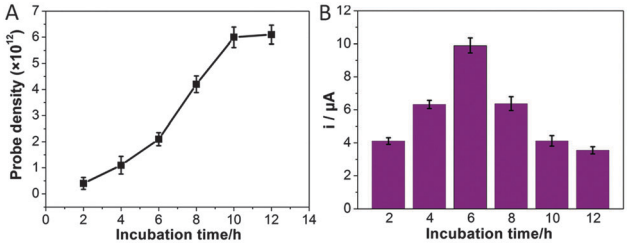

Fig. 5 (A) Probe density on the surface of the GNA incubated with 5 μM capture probes for 2 h, 4 h, 6 h, 8 h, 10 h, and 12 h. (B) Effect of the probe density on the signal response in the presence of 1 nM Tob.

oligonucleotide strands, resulting in a large electron-transfer resistance (curve d). However, when the Tob was added, the formed Apt-T–Tob complex was disassociated from the electrode surface, leading to an apparent decrease in the impedance semicircle (curve e). Finally, the Rp-T–AuNPs were introduced into the detection system, and significantly improved steric hindrance and electrostatic repulsion were produced at the interface, resulting in remarkably increased resistance (curve f).

Moreover, CVs were recorded to monitor the current response (i) during the detection of Tob. In the absence of Tob, merely a smooth cyclic curve was obtained, which is shown as curve a in Fig. 4B. In contrast, when Tob of 1 nM concentration was added, a well-defined redox pair was observed (curve b in Fig. 4B), indicating that the designed sensing scheme is feasible in the detection of Tob.

Effect of optimization of experimental conditions on the signal responses

CC was applied to investigate the density of capture probes on the 3D GNA, and RuHex served as the electrochemical indicator in the CC experiments, which is stoichiometrically bound to the anionic phosphodiester backbone of the oligonucleotide and therefore quantitatively reflects the number of oligonucleotide strands on the surface.[44] The probe density (Γ_{ss}, molecules cm^{-2}) could be calculated from the following equation:

$$\Gamma_{ss} = (Q_{ss}\cdot N_A/nFA)(z/m)$$

Here, n is the number of electrons per molecule for reduction ($n = 1$), F is the Faraday constant (96 485 C mol^{-1}), A is the real area of the working electrode (A = 1.80 cm^2), m is the number of nucleotides in the capture probe (m = 27), z is the charge of the redox molecules (z = 3), N_A is Avogadro's number ($N_A = 6.02 \times 10^{23}$ mol^{-1}), and Q_{ss} is the net capacitive charge of the capture probes.

As shown in Fig. 5A, with the incubation time ranging from 2 to 10 h, the probe density increased from 4.0×10^{11} to 6.1×10^{12} molecules cm^{-2}. On further increasing the incubation time to 12 h, no obvious increment in the density was observed. Meanwhile, the effect of the resulting density on the signal response was explored in detail. As shown in Fig. 5B, a higher current signal (i) was observed with a proper incubation time of 6 h, in which the probe density was estimated to be *ca.* 2.1×10^{12} molecules cm^{-2}. It is known that a lower probe density usually led to the generation of weak signals, while a higher density resulted in increased steric hindrance,[45] which severely hindered the interactions between the aptamers and biological proteins.

In addition, high hybridization efficiency between the capture probes and Apt-T is required to obtain large signal changes in the presence of Tob, which is critical to realize an excellent sensing performance. Therefore, after the Apt-T was hybridized with capture probes for different times ranging from 1 to 5 h, the Rp-T–AuNPs were added and the corresponding signal responses were recorded. As shown in Fig. S2 in the ESI,† with increased hybridization time, more capture probes were hybridized with the Apt-T and the electrochemical signal arising from the Rp-T II was reduced. With a hybridization time over 3 h, the signal responses approached a stable and negligible level, indicating that in this condition nearly all of the available capture probes were coupled with the Apt-T. As a result, an optimized time of 3 h was introduced to ensure thorough hybridization between the capture probes and Apt-T.

Performance of the fabricated aptasensor

The sensitivity of the electrochemical aptasensor was investigated by varying the concentrations of Tob, and SWV was implemented to monitor the current change (Δi, the change of peak current before/after the addition of Tob).

As shown in Fig. 6A, the current signal (i) increased with increasing Tob concentration. The calibration curve shows a good linear relationship between Δi and the concentration of Tob (curve a in Fig. 6B), and a regression equation of $\Delta i = (24.67 \pm 0.82) + (1.68 \pm 0.08)\cdot\log(C_{Tob}/M)$ ($R^2 = 0.998$) was obtained. Based on the developed aptasensor, a wide linear range from 10 fM to 1 nM with an ultralow detection limit of 3 fM (calculated by $D_L = 3S_B/m$, where S_B is the standard deviation of the blank measures and m is the slope of the calibration curve obtained from the linear regression analysis) was realized.[46] Obviously, the large surface area of the 3D GNA significantly increased the number of immobilization sites for capture probes, and each gold nanowire of the 3D GNA was separated at a proper distance, facilitating the diffusion of the Tob molecules and making the electrode surface easily accessible to them. Both of these factors enhanced the acquisition of electrochemical signals and finally contributed to an impressive detection limit of 3 fM. The detectable concentration of Tob in the present work was comparable to those reported in most of the literature (typically 0.12 pM to 3 nM, shown in Table S1

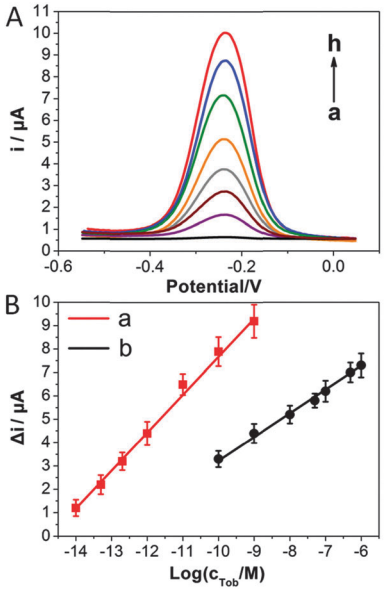

Fig. 6 (A) SWV responses of the proposed aptasensor after incubating with Tob at different concentrations (from curve a to h: 0 fM, 10 fM, 50 fM, 200 fM, 1 pM, 10 pM, 100 pM and 1 nM). (B) Calibration curves for the detection of Tob based on (a) the 3D GNA, (b) the bare gold electrode.

in the ESI†).[7,47–52] In addition, a similar detection of Tob based on the bare gold electrode was also investigated. Under the same experimental conditions, a higher detection limit of *ca.* 50 pM was observed (curve b in Fig. 6B). It should be noted that the sensitivity of the 3D GNA-based aptasensor was over 3 orders of magnitude higher than that of the bare gold electrode, confirming that the significantly enhanced surface area, high stability and favorable surface structure of the 3D GNA played a critical role in the ultrasensitive detection of Tob.

The selectivity, reproducibility and stability of the aptasensor

In addition to the sensitivity of an aptasensor, its selectivity, reproducibility and stability are also critical for its practical applications. The selectivity of the aptasensor was determined by challenging it with 1 pM Tob, 1 mM Lzm, 1 mM Hb, 1 mM BSA, 1 mM IgG and a mixture of these. As shown in Fig. 7, the aptasensor exhibited almost negligible responses to other proteins compared with that to 1 pM Tob. The results showed that the fabricated aptasensor possesses an excellent selectivity to Tob over other biological proteins, attributed to the highly specific interaction between the Apt-T and Tob.

To investigate the reproducibility of the aptasensor, five freshly prepared aptasensors were incubated with 1 pM Tob. All five samples exhibited similar signal responses, and the relative standard deviation (RSD) was estimated at around 4.6% (Fig. S3A in the ESI†). This demonstrated that the reproducibility of the proposed aptasensor is satisfactory.

Furthermore, the aptasensor was first stored in the refrigerator at 4 °C for 1 week, 2 weeks and 3 weeks, and then examined after adding Tob and Rp-T–AuNPs. The results of the experiments showed that the aptasensor retained *ca.* 92.6% of its initial response even after 3 weeks (Fig. S3B in the ESI†), indicating that the stability of the fabricated aptasensor is acceptable.

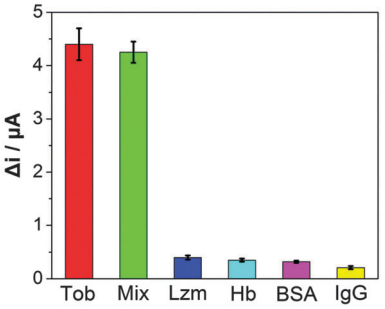

Fig. 7 Selectivity evaluation of the proposed aptasensor for 1 pM Tob against 1 mM Lzm, 1 mM Hb, 1 mM BSA, 1 mM IgG and a mixture of these.

Table 1 Analytical results for Tob detection in a human serum sample

Samples	Added	Detected	Recovery (%)	RSD (%)
1	100 fM	99.8 fM	99.8	4.8
2	1.00 pM	1.01 pM	101	4.4
3	10.0 pM	10.2 pM	102	3.9
4	50.0 pM	49.7 pM	99.4	4.0
5	100 pM	99.9 pM	99.9	3.6

Practical applications of the aptasensor

Owing to the preeminent sensitivity and selectivity of our proposed aptasensor, here we assess the performance of this aptasensor to determine Tob in real human serum. The blank human serum was first screened according to the obtained calibration curve, and no Tob was found. The standard addition method was then employed to evaluate the applicability of the aptasensor. The analytical results are shown in Table 1. From Table 1, we can see that the recovery (between 99.4% and 102%) and RSD (between 3.6% and 4.8%) are satisfactory, which distinctly indicates that the aptasensor has promising potential for Tob detection in real biological samples.

Conclusions

In this work, *in situ* prepared DAAQ nanowires were proven to be a promising and reliable template for the fabrication of array structures. As an example, a 3D GNA with significantly enhanced surface area, pure components, high stability and a favorable surface structure was successfully constructed, and this could serve as a suitable candidate in electrochemical sensing. As a result, an ultrasensitive electrochemical Tob aptasensor was designed on the 3D GNA, in which an ultralow detection limit, as well as excellent selectivity, good reproducibility and high stability, was observed. The proposed aptasensor also showed potential for application in the analysis of real serum samples. We expect that the developed DAAQ template could be employed for fabricating more nanowire arrays, and the proposed 3D GNA will have great promise in constructing more ultrasensitive and selective electrochemical biosensors.

Acknowledgements

This work was supported by the Innovative Research Team Program by the Ministry of Education of China (No. IRT13070), the Doctoral Fund of the Ministry of Education of China (No. 20113221110001) and a project was funded by the Priority Academic Program Development of Jiangsu Higher Education Institutions (PAPD).

Notes and references

1 A. A. Lubin and K. W. Plaxco, *Acc. Chem. Res.*, 2010, **43**, 496–505.
2 J. Liu, Z. Cao and Y. Lu, *Chem. Rev.*, 2009, **109**, 1948–1998.
3 W. Tan, M. J. Donovan and J. Jiang, *Chem. Rev.*, 2013, **113**, 2842–2862.
4 P. Hu, C. Zhu, L. Jin and S. Dong, *Biosens. Bioelectron.*, 2012, **34**, 83–87.
5 H. Huang, Y. Tan, J. Shi, G. Liang and J. J. Zhu, *Nanoscale*, 2010, **2**, 606–612.
6 Z. Zhang, S. Liu, Y. Shi, Y. Zhang, D. Peacock, F. Yan, P. Wang, L. He, X. Feng and S. Fang, *J. Mater. Chem. B*, 2014, **2**, 1530–1538.
7 J. Chen, X. Jiao, H. Luo and N. Li, *J. Mater. Chem. B*, 2013, **1**, 861–864.
8 B. Kavosi, A. Salimi, R. Hallaj and K. Amani, *Biosens. Bioelectron.*, 2014, **52**, 20–28.
9 Y. Peng, D. Zhang, Y. Li, H. Qi, Q. Gao and C. Zhang, *Biosens. Bioelectron.*, 2009, **25**, 94–99.
10 L. Bai, R. Yuan, Y. Chai, Y. Zhuo, Y. Yuan and Y. Wang, *Biomaterials*, 2012, **33**, 1090–1096.
11 L. Shi, Z. Chu, Y. Liu, J. Peng and W. Jin, *J. Mater. Chem. B*, 2014, **2**, 2658–2665.
12 H. X. Chang, L. H. Tang, Y. Wang, J. H. Jiang and J. H. Li, *Anal. Chem.*, 2010, **82**, 2341–2346.
13 S. Zhu, S. Han, L. Zhang, S. Parveen and G. Xu, *Nanoscale*, 2011, **3**, 4589–4592.
14 B. F. Ye, Y. J. Zhao, Y. Cheng, T. T. Li, Z. Y. Xie, X. W. Zhao and Z. Z. Gu, *Nanoscale*, 2012, **4**, 5998–6003.
15 J. S. Lee, S. G. Kim, J. Jun, D. H. Shin and J. Jang, *Adv. Funct. Mater.*, 2014, **24**, 6145–6153.
16 I. Willner and M. Zayats, *Angew. Chem., Int. Ed.*, 2007, **46**, 6408–6418.
17 X. J. Huang, A. M. O'Mahony and R. G. Compton, *Small*, 2009, **5**, 776–788.
18 A. Walcarius, S. D. Minteer, J. Wang, Y. Lin and A. Merkoci, *J. Mater. Chem. B*, 2013, **1**, 4878–4908.
19 L. Shi, Z. Chu, X. Dong, W. Jin and E. Dempsey, *Nanoscale*, 2013, **5**, 10219–10225.
20 K. Saha, S. S. Agasti, C. Kim, X. Li and V. M. Rotello, *Chem. Rev.*, 2012, **112**, 2739–2779.
21 L. P. Xu, S. Wang, H. Dong, G. Liu, Y. Wen, S. Wang and X. Zhang, *Nanoscale*, 2012, **4**, 3786–3790.
22 L. Shi, Z. Chu, Y. Liu, W. Jin and X. Chen, *Biosens. Bioelectron.*, 2013, **49**, 184–191.
23 A. Andreu, J. W. Merkert, L. A. Lecaros, B. L. Broglin, J. T. Brazell and M. El-Kouedi, *Sens. Actuators, B*, 2006, **114**, 1116–1120.
24 X. Zhang, D. Li, L. Bourgeois, H. Wang and P. A. Webley, *ChemPhysChem*, 2009, **10**, 436–441.
25 J. Xu, F. Shang, J. H. T. Luong, K. M. Razeeb and J. D. Glennon, *Biosens. Bioelectron.*, 2010, **25**, 1313–1318.
26 M. Yang, F. Qu, Y. Li, Y. He, G. Shen and R. Yu, *Biosens. Bioelectron.*, 2007, **23**, 414–420.
27 S. Cherevko and C. Chung, *Sens. Actuators, B*, 2009, **142**, 216–223.
28 S. Samanman, C. Thammakhet, P. Kanatharana, C. Buranachai and P. Thavarungkul, *Electrochim. Acta*, 2013, **102**, 342–350.
29 J. Byun, J. Lee, S. Kwon, G. Jeon and J. Kim, *Adv. Mater.*, 2010, **22**, 2028–2032.
30 T. S. Ramulu, R. Venu, B. Sinha, B. Lim, S. J. Jeon, S. S. Yoon and C. G. Kim, *Biosens. Bioelectron.*, 2013, **40**, 258–264.
31 W. Ruf and B. M. Mueller, *Semin. Thromb. Hemostasis*, 2006, **32**, 61–68.
32 Y. L. Chen, C. Y. Lee and H. T. Chiu, *J. Mater. Chem. B*, 2013, **1**, 186–193.
33 J. Zhao, Y. Zhang, H. Li, Y. Wen, X. Fan, F. Lin, L. Tan and S. Yao, *Biosens. Bioelectron.*, 2011, **26**, 2297–2303.
34 D. K. Lahiri and B. Schnabel, *Biochem. Genet.*, 1993, **31**, 321–328.
35 J. Zhang, S. Song, L. Wang, D. Pan and C. Fan, *Nat. Protoc.*, 2007, **2**, 2888–2895.
36 Y. S. Zhao, J. Wu and J. Huang, *J. Am. Chem. Soc.*, 2009, **131**, 3158–3159.
37 C. Gao, Q. Zhang, Z. Lu and Y. Yin, *J. Am. Chem. Soc.*, 2011, **133**, 19706–19709.
38 A. A. Karyakin, E. A. Puganova, I. A. Bolshakov and E. E. Karyakina, *Angew. Chem., Int. Ed.*, 2007, **46**, 7678–7680.
39 S. Guo, L. Wang and E. Wang, *Chem. Commun.*, 2007, 3163–3165.
40 S. Trasatti and O. A. Petrii, *Pure Appl. Chem.*, 1991, **63**, 711–734.
41 C. Fan, K. W. Plaxco and A. J. Heeger, *Proc. Natl. Acad. Sci. U. S. A.*, 2003, **100**, 9134–9137.
42 Z. Tang, P. Mallikaratchy, R. Yang, Y. Kim, Z. Zhu, H. Wang and W. Tan, *J. Am. Chem. Soc.*, 2008, **130**, 11268–11269.
43 X. Chen, Y. Wang, J. Zhou, W. Yan, X. Li and J. J. Zhu, *Anal. Chem.*, 2008, **80**, 2133–2140.
44 A. B. Steel, T. M. Herne and M. J. Tarlov, *Anal. Chem.*, 1998, **70**, 4670–4677.
45 J. Zhang, S. Song, L. Zhang, L. Wang, H. Wu, D. Pan and C. Fan, *J. Am. Chem. Soc.*, 2006, **128**, 8575–8580.
46 G. L. Long and J. D. Winefordner, *Anal. Chem.*, 1983, **55**, 712A–724A.
47 A. Sun, Q. Qi, X. Wang and P. Bie, *Biosens. Bioelectron.*, 2014, **57**, 16–21.
48 H. Fan, H. Li, Q. Wang, P. He and Y. Fang, *Biosens. Bioelectron.*, 2012, **35**, 33–36.
49 F. Yan, F. Wang and Z. Chen, *Sens. Actuators, B*, 2011, **160**, 1380–1385.
50 L. Shi, Z. Chu, Y. Liu, W. Jin and N. Xu, *Adv. Funct. Mater.*, 2014, **24**, 7032–7041.
51 L. Bai, Y. Chai, R. Yuan, Y. Yuan, S. Xie and L. Jiang, *Biosens. Bioelectron.*, 2013, **50**, 325–330.
52 X. He, G. Wang, G. Xu, Y. Zhu, L. Chen and X. Zhang, *Langmuir*, 2013, **29**, 14328–14334.

